AIP | Applied Physics Letters

Dynamics of capillary self-alignment for mesoscopic foil devices

Gari Arutinov, Massimo Mastrangeli, Edsger C. P. Smits, Herman F. M. Schoo, Jürgen Brugger et al.

Citation: Appl. Phys. Lett. **102**, 144101 (2013); doi: 10.1063/1.4801088
View online: http://dx.doi.org/10.1063/1.4801088
View Table of Contents: http://apl.aip.org/resource/1/APPLAB/v102/i14
Published by the American Institute of Physics.

Dynamics of capillary self-alignment for mesoscopic foil devices

Gari Arutinov,[1,2] Massimo Mastrangeli,[3] Edsger C. P. Smits,[1] Herman F. M. Schoo,[1] Jürgen Brugger,[3] and Andreas Dietzel[4]
[1]*Holst Center/TNO, High Tech Campus 31, 5656AE, Eindhoven, The Netherlands*
[2]*Micro- and Nano-Scale Engineering Section (MNSE), Eindhoven University of Technology, Eindhoven, The Netherlands*
[3]*Microsystems Laboratory, École Polytechnique Fédérale de Lausanne (EPFL), Lausanne, Switzerland*
[4]*Technische Universität Braunschweig, Institut für Mikrotechnik, Langer Kamp 8, 38106 Braunschweig, Germany*

(Received 5 February 2013; accepted 23 March 2013; published online 9 April 2013)

We report experimental evidence for three sequential, distinct dynamic regimes in the capillary self-alignment of centimeter-sized foil dies released at large uniaxial offsets from equilibrium. We show that the initial transient wetting regime, along with inertia and wetting properties of the dies, significantly affect the alignment dynamics including the subsequent constant acceleration and damped oscillatory regimes. An analytical force model is proposed that accounts for die wetting and matches quasi-static numerical simulations. Discrepancies with experimental data point to the need for a comprehensive dynamical model to capture the full system dynamics. © *2013 American Institute of Physics*. [http://dx.doi.org/10.1063/1.4801088]

Capillary self-alignment (SA) is an innovative assembly technique,[1] where the relaxation of carefully confined liquid droplets is used to register micro[2]- and meso-scopic[3] parts, normally dies, onto patterned substrates. The configuration minimizing the system energy coincides with the alignment of the dies onto matching binding sites within tolerances[2] adequate for precision fabrication. Capillary SA can complement pick-and-place assembly approaches to overcome their performance trade-offs.[4] Several groups have modeled[5] and demonstrated[6,7] the accuracy and repeatability of the technique. Conversely, only few studies have addressed the lateral dynamics of the alignment process[8] and, to our knowledge, only for (sub-) millimetric dies where the Bond numbers are much smaller.

We investigated the dynamics of lateral capillary SA of centimeter-sized foil dies (Fig. 1(a))—a process we recently demonstrated.[9] A set of 18×18 mm^2 foil dies were self-aligned onto matching, silicon dioxide binding sites patterned on test substrates. The optically transparent polyethylene naphthalate (PEN) dies and Au-coated Si substrates were fabricated and marked with laser-etched measuring structures as detailed previously.[9] The dies were handled through a home-built micropositioning stage equipped with integrated vacuum tweezers (SMD-VAC-HP, Vacuum Industries, Inc.). A positioning base stage (XYZ 500 TIS, Quater Research and Development) providing 10 μm-resolved displacements along three axes was used to pre-align the dies. The full alignment dynamics was tracked by a high-speed camera (Redlake HS-3) combined with a microscope stage and analyzed through image recognition software. The dynamics of the water triple contact line was concurrently tracked by focusing the camera on the outer edge of the dies (Fig. 1(b)).

A 125 μm-thick water layer was dispensed on the binding sites through micropipettes. The thickness h and the surface tension γ of the liquid layer directly affect the lateral capillary forces driving the alignment process.[10] The thickness of the water layer was calculated from the dispensed water volume and the area of the sites. It was optimized to consistently achieve accurate registration of the dies upon SA ($\approx$30 μm, as limited by laser dicing tolerance, to be compared with the centimetric dies dimensions).[9]

Shortly after water dispensing, the dies were pre-aligned with edges parallel to those of the binding sites and with predefined offsets $\{u\}$ along one of the axes (principal) of the sites, while held at 225 ± 25 μm above the water layer. All initial offsets were much larger than the thickness of the lubricant layer (i.e., $\{u\} \gg h$). The initial offset along the perpendicular (secondary) axis was negligible when not enforced otherwise. The axial offset was defined as the distance between the releasing and the target positions of the dies. The procedure was repeated for every experiment. All experiments were repeated 5 times. Quantitative analysis of repeatability and accuracy of the capillary self-alignment process were reported in our previous publication.[9] Here, we focus on typical cases.

Upon release from the tweezers, the dies landed on top of the water layer with unnoticeable lateral deviation from the predefined offset. Starting from such initial overlap with the water layer, a die's uniaxial trajectory evidenced three distinct dynamical regimes (Fig. 2(a)). During *transient wetting*, the die remained at rest while the underlying water layer deformed as it progressively wetted the die's bottom surface. The ensuing meniscus pinned to all edges of the die's bottom surface except to its outer one (Fig. 1(b)). The impact of the die on the free water surface caused its impulsive deformation and inhomogeneous spreading of the unpinned triple contact line (see supplementary material for related videos).[4] In all experiments, the formation and evolution of the meniscus upon contact with the die completed before the inception of lateral die translation. Remarkably, at this stage wetting of the full bottom die surface by the meniscus was never achieved. The meniscus then started pulling the die sideways. Lateral die traction is the joint effect of: (1) the relaxation of the water meniscus toward the

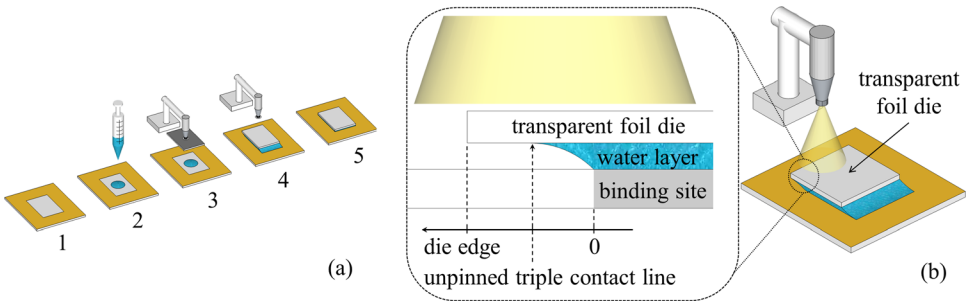

FIG. 1. (a) Process steps for capillary SA of a foil die: (1) patterning of the carrier substrate,[9] (2) deposition of water droplet, (3) coarse die pre-alignment, (4) die release and meniscus formation, (5) die self-alignment on binding site. (b) Concurrent high-speed tracking of uniaxial lateral capillary SA and water triple contact line dynamics (see Fig. 4). The camera was focused on the outer edge of the transparent foil die (not to scale).

equilibrium geometry defined by its boundary conditions; and (2) the concurrent sliding motion of the die self-centering on top of the meniscus. In this second regime, the die moved with *constant acceleration* describing a parabolic 1D trajectory (Figs. 2(a) and 2(b)). Around the time the die first crossed its target position, the outer die edge reached the unpinned triple contact line of the meniscus—i.e., only then was full wetting observed. As shown later, line pinning was conditional to the foil's surface energy. Lastly, for $u \approx h$, the die started undergoing *harmonic oscillatory motion* underdamped by dissipative viscous forces (Fig 2(a)).[8] The die finally settled in accurate registration with its binding site.[9]

The initial offset and the fluid mechanics of the contact between die and liquid layer are critical for capillary SA performance.[7,11] Still, the formation and initial evolution of the liquid bridge upon contact with the die so far received little attention. In fact, wetting of the bottom die surface is either not controlled, as in most experiments,[7] or assumed to be complete, as in both static[5] and dynamic[8] models. Such modeling assumption comes along with two additional ones: one explicit, i.e., relatively small displacements of the die from its rest position (i.e., $\{u\} \approx h$); and one implicit, i.e., the die being displaced to initial non-null offsets *from* the equilibrium position. The additional assumptions do not evidently hold in our case. As reported below, our data show that we do *not* observe full die wetting, while in earlier studies on micrometric dies[7] this was assumed to be the case. Here this could be studied in detail thanks to the transparency and the dimensions of our vehicles, which allowed for a separation

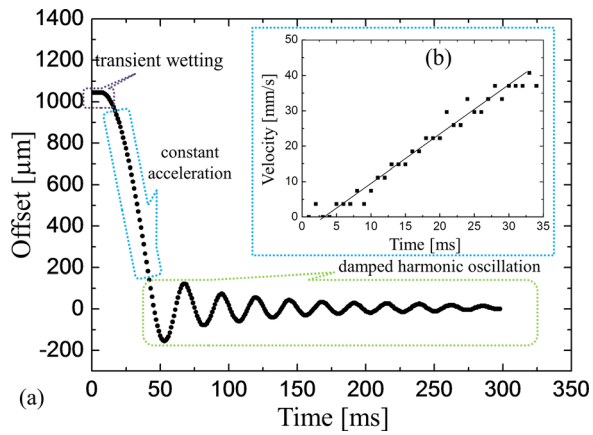

FIG. 2. (a) Typical self-alignment trajectory of a foil die (0.80 mg/mm^2). Data extracted from high-speed video recording starting upon die contact with water. The three regimes (transient wetting, constant acceleration and damped oscillation) are evidenced. (b) Numerical derivative of the parabolic regime depicted in (a) showing the linear progression of velocity in time.

of timescales between initial meniscus formation and die motion inception.

We assumed that the surface energy of the foil dies could impact the formation of the water meniscus and the consequent SA dynamics. We therefore tailored the degree of wettability of the foil dies. Water contact angle (CA) on bare PEN foil was $65° \pm 3°$ ($4 \pm 2°$ for the silicon dioxide sites), as measured by the static sessile drop method. A 100 nm layer of silicon nitride (referred as SiN) was deposited via plasma-enhanced chemical vapor deposition (PECVD) on bare PEN foils. Subsequent exposure of the SiN-coated foil dies to O_2 plasma at 400 W for 1 min increased their surface energy, decreasing the water CA to $9° \pm 2°$. Alternatively, a perfluorodecyltriethoxysilane ($C_{16}H_{19}F_{17}O_3Si$, 97%, Sigma-Aldrich) self-assembled monolayer (SAM) was adsorbed from vapor phase for 30 min at 120 °C on the O_2 plasma-activated SiN surfaces, increasing their water CA to $98° \pm 3°$. None of these treatments visibly affected the optical transparency of the dies.

Data analysis showed significant differences in SA dynamics as a function of the degree of wettability of the dies (see Fig. 3). For all the wetting degrees investigated, full wetting of the bottom die surface by the water meniscus was never achieved during the first regime. As expected, the spreading of the water triple contact line across the die (equivalently, the fraction of the bottom die surface not wet by water) was proportional (inversely proportional) to the wettability of its bottom surface (see supplementary material for analysis of recorded SA dynamics).[4] Moreover, the duration of the transient wetting regime was inversely proportional to the surface energy of the die. More wettable dies started moving sideways earlier and first crossed their target position in shorter times.

For hydrophilic dies, after initial spreading the unpinned water contact line did not change its profile till the die had reached close proximity of its target position. Only by that time the outer edge of the die had converged to the position of the water contact line. Upon consequent pinning, the water contact line (red line in Fig. 3(a)) and die edge (black line) moved solidly. Untreated PEN dies induced a similar behavior, except for a considerably smaller initial spreading of the water contact line that could barely be resolved by our setup (Fig. 3(b)). Conversely, no spreading of the water contact line could be detected for the hydrophobic dies. In this case, the water contact line could also be clearly seen unpinning from the outer die edge during its backtracking motion, whereas it was pinned to it during the remainder of the oscillation periods (Fig. 3(c)).

Quasi-static simulations performed by Surface Evolver (SE)[12] predicted the partial wetting of the mesoscopic dies

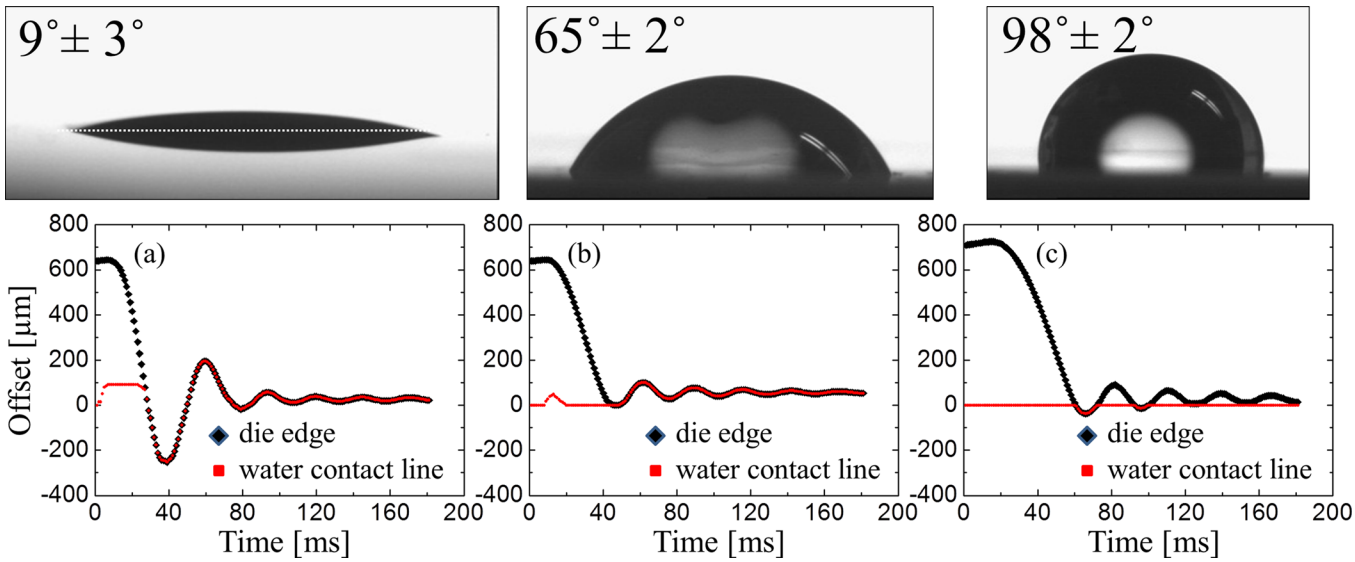

FIG. 3. Uniaxial lateral alignment dynamics of a foil die and water contact line dynamics tracked as sketched in Fig. 1(b) (die: 0.80 mg/mm^2; initial offset 650 ± 30 μm). Trajectories for the case of hydrophilic die (a), untreated die (b) and hydrophobic die (c). Null offset coincides with the closer edge of the underlying binding site, i.e., with the position of the edge of the unperturbed water layer. For case (c), the displacement of the water contact line could not be resolved by the camera when the line was not pinned to the outer edge of the die.

by the meniscus upon water-to-die contact. However, the simulated die surface S_{SE}, not wet by the meniscus underestimates experimental results S_{exp} (e.g., $S_{SE} = 1.6$ mm^2 and $S_{exp} = 11.5$ mm^2 for hydrophilic foil dies ($S_{die} = 324$ mm^2)). This may be due to non-idealities (e.g. roughness, chemical inhomogeneity) of the die surface, leading to contact angle hysteresis and contact line pinning.[13] This is supported by the mentioned inhomogeneous perturbation of the contact line during transient wetting (see supplementary material for related video).[4]

The degree of wettability of the die affects the second regime of the dynamics as well (Fig. 4). In this regime, the constant acceleration of the die appeared proportional to the surface energy (Fig. 4(b)). Accordingly, during this regime a constant, surface energy-dependent shearing force acts on the foil die. This force is a combination of a lateral capillary force, driving the die toward its binding site, with an opposing dissipative force due to the viscosity and aspect ratio of the underlying, thin water layer.

The dissipative viscous force was estimated using Newton's law of viscosity assuming a linear vertical velocity gradient within the liquid layer.[14] The estimated value ($F_{fric} = 28 \pm 5$ μN; see supplementary material for detailed calculation),[4] assumed equal for the three wettability cases, amounts to a small fraction of the net measured lateral force (e.g., $F_{net} = 468 \pm 37$ μN for hydrophobic foil dies) (Fig. 4(b)). Consequently, capillary action appears dominant in the second regime. For large displacements from equilibrium, lateral capillary forces were computed numerically through SE simulations, as well as analytically using a *sliding* model: $F_{cap} = -L\gamma(1 + cos\theta)$ (for θ the CA of water). The sliding model accounts for wetting and contact line unpinning, and it well matches the quasi-static predictions of SE; yet both models substantially overestimate experimental data (see supplementary material for model derivation and results).[4]

The dies used in this study had a Bond number $Bo = \rho g L^2/\gamma = 43.6 \gg 1$. In contrast to the sub-millimetric case, the inertia of the considered dies was thus expected to significantly affect their SA dynamics as compared to the capillary forces, particularly in the oscillatory regime. To investigate this, PEN dies with different thicknesses leading

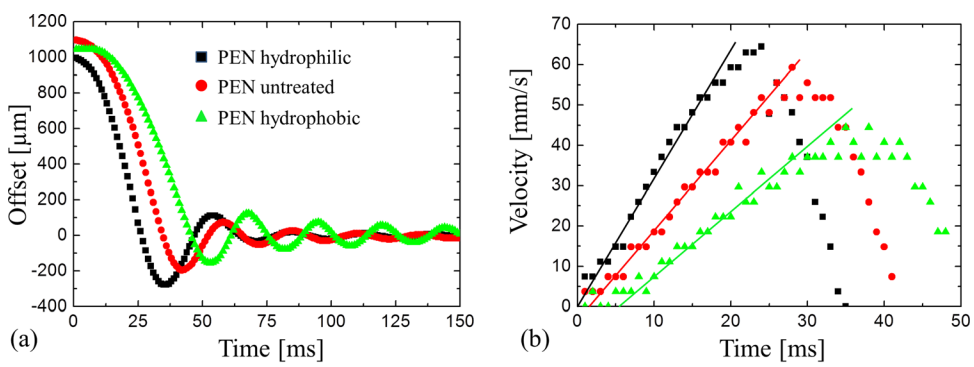

	Acceleration [mm/s^2]	Force [μN]
PEN hydrophilic	3.25	870
PEN untreated	2.45	656
PEN hydrophobic	1.75	468

FIG. 4. (a) Self-alignment trajectories and (b) corresponding linear increase of velocity in time during the parabolic regime for a foil die (0.80 mg/mm^2) as function of different degrees of wettability parameterized by water CAs. Corresponding accelerations and net forces obtained from acquired data and foil masses are shown in the inset table. Data noise in (b) mainly attributed to the numerical computation of the derivative of the data in (a).

to a range of mass densities varying from 0.18 to 0.98 mg/mm^2 were pre-aligned over corresponding binding sites with pre-fixed initial offset of 950 ± 50 μm. Analysis of their recorded SA trajectories evidenced a clear impact of inertial effects on the third dynamical regime (Fig. 5). Notably, in this case, the experimental data could also be benchmarked rather accurately against SE simulations (see Table in Fig. 5).

Finally, we observed that the lateral alignment dynamics of a square-shaped foil die along the principal axis is barely affected by a smaller offset (e.g., positioning error) along the secondary axis. A foil die (0.80 mg/mm^2) was repeatedly released at different, prefixed offsets along the secondary axis while the initial offset along the principal axis was kept constant within loading precision. The corresponding SA data revealed no divergence of the trajectories along the principal axis during the second regime (Fig. 6(a)) in spite of large differences in the dynamics along the secondary axis (Fig. 6(b)). Remarkably, the initial offset along the secondary axis was not necessarily the largest to be reached in time by the die along that same axis, which is instead never the case for the principal. This represents evidence of energy transfer between the degenerate resonance modes associated with the coordinated axes of the square sites. Trajectory divergence along the principal axis was instead observed during the oscillatory regime. This depends on differences in initial offsets, but may also point to weak coupling between the degenerate modes for comparable oscillation amplitudes. Further studies are being pursued to follow up on this issue.

In conclusion, this letter reports insights into the dynamics of capillary self-assembly for mesoscopic foil dies. We established that for foil dies, released from uniaxial non-equilibrium positions of large offset above matching binding sites, the ensuing dynamics unfolds into three distinct dynamic regimes. Our experimental data question some basic assumptions of common models of the process, mainly the full wetting of the die surface by the fluid meniscus upon initial contact. The wettability and the inertia of the dies were also shown to impact the alignment dynamics. Conversely, the unsatisfactory match between calculated and measured force data remarked the limitations of analytical models of dynamics. A comprehensive, numerical dynamic model—accounting for wetting, triple contact line dynamics and contact angle hysteresis in addition to meniscus geometry and capillary action—seems therefore necessary to capture the full experimental details of the process. Our insights provide deeper understanding of the capillary SA process for the assembly of mesoscopic functional foil-based devices, such as sensor foils, paper batteries and radio-frequency identification (RFID), which are being introduced in a variety of relevant technological and commercial applications.[15]

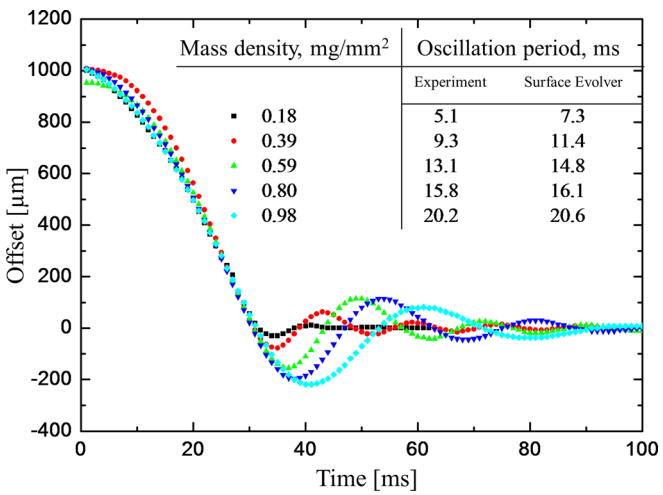

FIG. 5. Self-alignment trajectories of foil dies with different mass densities (shown in inset), and corresponding oscillation periods as extracted from experimental trajectories as well as from SE simulations of quasi-static resonance frequencies (shown in inset).

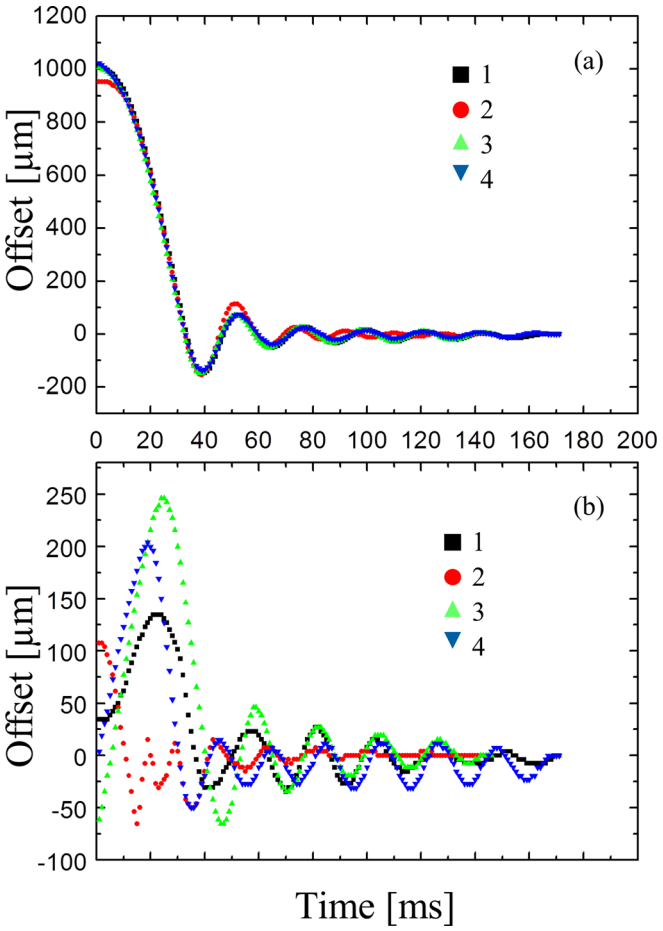

FIG. 6. Self-alignment trajectory of a foil (0.80 mg/mm^2) die as recorded by high-speed camera along (a) principal and (b) secondary axis. The die was repeatedly released at various initial offsets along the secondary axis, while initial offsets along main axis was kept the same within loading precision of the micropositioner.

This work was funded through the Marie Curie ITN FlexSmell project No. 238454 and the Nano-Tera.ch research initiative within the context of the SelfSys project. The authors would like to thank G. van Heck for laser processing, B. van Remoortere for foil lamination experiments, T. Geuns for lithographical patterning of silicon wafers and F. van Assche for PECVD deposition of SiN.

[1]N. B. Crane, O. Onen, J. Carballo, Q. Ni, and R. Guldiken, Microfluid. Nanofluid. **14**, 383 (2013).
[2]U. Srinivasan, D. Liepmann, and R. T. Howe, Microelectromech. Syst. J. **10**(1), 17 (2001).

[3]C. Landesberger, E. Yacoub-George, W. Hell, and K. Bock, presented at the Electronic System-Integration Technology Conference (ESTC), 2010 3rd (Berlin, Germany, 2010).
[4]See supplementary material at http://dx.doi.org/10.1063/1.4801088 for full model derivation and self-alignment videos.
[5]J. Berthier, K. Brakke, F. Grossi, L. Sanchez, and L. Di Cioccio, J. Appl. Phys. **108**(5), 054905 (2010).
[6]T. Fukushima, E. Iwata, T. Konno, J. C. Bea, K. W. Lee, T. Tanaka, and M. Koyanagi, Appl. Phys. Lett. **96**(15), 154105 (2010).
[7]V. Sariola, M. Jaaskelainen, and Q. A. Zhou, IEEE Trans. Robot. **26**(6), 965 (2010).
[8]P. Lambert, M. Mastrangeli, J. B. Valsamis, and G. Degrez, Microfluid. Nanofluid. **9**(4–5), 797 (2010).
[9]G. Arutinov, E. C. P. Smits, M. Mastrangeli, G. van Heck, J. van den Brand, H. F. M. Schoo, and A. Dietzel, J. Micromech. Microeng. **22**(11), 115022 (2012).
[10]M. Mastrangeli, J.-B. Valsamis, C. Van Hoof, J.-P. Celis, and P. Lambert, J. Micromech. Microeng. **20**(7), 075041 (2010).
[11]K. Sato, K. Ito, S. Hata, and A. Shimokohbe, Precis. Eng.-J. Int. Soc. Precis. Eng. Nanotechnol. **27**(1), 42 (2003).
[12]K. Brakke, in *Experimental Mathematics* (1992), Vol. 1, pp. 141.
[13]V. E. B. Dussan, "On the spreading of liquids on solid surfaces: Static and dynamic contact lines," Annu. Rev. Fluid. Mech. **11**, 371 (1979).
[14]N. van Veen, J. Electron. Packag. **121**(2), 116 (1999).
[15]D. Briand, A. Oprea, J. Courbat, and N. Bârsan, Mater. Today **14**(9), 416 (2011).